

High-temperature polymorph of In_2La

E.R. Nieuwenhuis, Gary S. Collins*, Aurélie Favrot, Matthew O. Zacate

Department of Physics, Washington State University, Pullman, WA 99164-2814, USA

Received 31 May 2004; accepted 15 June 2004

Abstract

A polymorph of In_2La was discovered by observing a change in the quadrupole interaction at nuclei of $^{111}\text{In}/\text{Cd}$ probe atoms at high temperature using the technique of perturbed angular correlation of gamma rays. Point-symmetry information from the measured electric field gradient and chemical considerations suggests that the high-temperature polymorph has the hexagonal AlB_2 structure. The transformation between the low-temperature phase, which has the CeCu_2 structure, and the high-temperature phase takes place with hysteresis over a temperature range from 200 to 450 °C.

© 2004 Elsevier B.V. All rights reserved.

Keywords: Crystal structure and symmetry; Phase diagram; Intermetallics; X-ray and γ -ray spectroscopies

1. Introduction

According to the In–La phase diagram [1], six intermetallic compounds are stable at room temperature. X-ray diffraction measurements determined that In_2La has the orthorhombic CeCu_2 structure at room temperature [2], and it is shown in the phase diagram to be stable up to the melting point. In the course of a study of the neighboring In_3La phase [3] using the method of perturbed angular correlation of gamma rays (PAC), a high-temperature polymorph of In_2La was discovered that was characterized more completely through additional PAC measurements described in this paper.

2. Sample preparation

In_2La samples were prepared by melting foils of In (99.999% pure) and La (99.9% pure, REM basis) with carrier free ^{111}In under argon in an arc furnace. Extensive measurements were made on two samples having final masses of 27 mg and 83 mg, with compositions 33_{-3}^{+2} and

33_{-4}^{+3} at.% La. The stated uncertainties in composition reflect mass losses during melting and were calculated by assuming that decreases in mass were due entirely to the loss of one element or the other.

In_2La is known to oxidize rapidly [2]. It was determined in this laboratory to decompose into La_2O_3 and pure In as follows. Samples left in contact with air at room temperature showed a decrease of the PAC signal fraction for In_2La and a corresponding increase of a signal known to be due to In metal [4], indicating that La was lost from the In–La system. At the same time, a mass increase was observed that is quantitatively consistent with formation of La_2O_3 . Powder X-ray diffraction measurements at elevated temperature were attempted but were unsuccessful due to rapid reaction with residual oxygen in the diffractometer. On the other hand, ingots of In_2La could be studied conveniently using PAC without detectable oxidation over a period of weeks under a pressure of 5 μPa in a measurement oven.

3. Experimental method

The point symmetry at the site occupied by a PAC probe atom can be partially determined through the nuclear quadrupole interaction. In this study, a phase transformation

* Corresponding author.

E-mail address: collins@wsu.edu (G.S. Collins).

was detected through a change in point symmetry at $^{111}\text{In}/\text{Cd}$ probes. ^{111}In decays to an excited state of Cd via electron capture. The Cd nucleus subsequently emits two γ -rays in succession with energies 171 and 245 keV. In between the γ -emissions, the nucleus is in a long-lived intermediate state with spin 5/2 and a half-life of 85 ns. The electric field gradient (EFG) due to charges in the crystal surrounding the probe nucleus interacts with the nuclear quadrupole moment Q , causing the populations of magnetic substates to evolve. This leads to a time-dependent angular correlation of the second γ -ray with respect to the first that can be measured and is characterized by a perturbation function $G_2(t)$. For further information about the PAC technique, see references [5,6].

The EFG at a nucleus is the second derivative of the electrostatic potential due to extranuclear charges. The EFG is a traceless, second-order tensor V_{ij} that, when diagonalized, is fully described by its principal component V_{zz} and an asymmetry parameter $\eta \equiv (V_{xx} - V_{yy})/V_{zz}$. Partial information about point symmetry comes from the observed values of V_{zz} and η . For sites having cubic symmetry, $V_{zz} = 0$; for sites having a unique axis with 3-, 4- or 6-fold rotational symmetry, $V_{zz} \neq 0$ and $\eta = 0$; and for sites having lower symmetry, $V_{zz} \neq 0$ and $0 < \eta \leq 1$.

The perturbation function $G_2(t)$ for spin 5/2 is

$$G_2(t) = s_0 + \sum_{n=1}^3 s_n \cos(\omega_n t) \exp\left(-\frac{1}{2} \left(\sigma \frac{\omega_n}{\omega_1} t\right)^{3/2}\right) \quad (1)$$

The frequencies ω_n are functions of the coupling frequency $\omega_0 = \frac{3\pi}{10} |eQV_{zz}|/h$ and η [7], and the amplitudes $s_0, s_1, s_2,$ and s_3 sum to one. The exponential factors account empirically for inhomogeneous broadening due to distant defects or lattice strains. Frequency distribution widths σ were small (<1 Mrad/s) in all measurements. In general, $\omega_3 = \omega_1 + \omega_2$. For cubic symmetry, all ω_n are zero and $G_2(t) = 1$, inde-

pendent of time. For $\eta = 0$, $\omega_2 = 2\omega_1$ and $\omega_1 = \omega_0$ whereas for $\eta > 0$, $\omega_1 \leq \omega_2 < 2\omega_1$ and $\omega_1 > \omega_0$. Analytic expressions for ω_n in terms of ω_0 and η when $\eta > 0$ can be found in reference [7]. In this study, we use ω_0 and η to identify signals and are not interested in specific values of V_{zz} .

When probes are in sites with different EFGs, the overall perturbation function is a superposition of functions for probes in each site:

$$G_2(t) = \sum_i f_i G_{2,i}(t) \quad (2)$$

in which the signal fraction f_i is the fraction of probe atoms in site i . As presented below, the signals observed in this study are identified with probes in different phases. In general, f_i is not the phase fraction [8]. However, in these experiments, in which the probe is a host element and the phases of interest have the same composition, f_i is equal to the phase fraction.

The perturbation function $G_2(t)$ was measured using a four-detector fast-slow spectrometer with samples mounted in a measurement oven under a pressure of about 5 μPa . Measurement time at each temperature was typically one day. Spectra were fitted using Eqs. (1) and (2) in order to obtain signal fractions and quadrupole interaction parameters ω_0 and η . When signal fractions were large ($>30\%$), all parameters were fitted freely. When signal fractions were smaller, one or more of S_1, S_2, S_3 and ω_1 were fixed to values obtained from fits of other spectra.

4. Results

Representative PAC spectra are shown on the left in Fig. 1. The spectrum measured at 10.6 °C (Fig. 1a) exhibits a low-temperature (LT) signal with $\omega_0 = 78.7(2)$ Mrad/s and $\eta = 0.317(1)$. The spectrum measured at 524.0 °C (Fig. 1c)

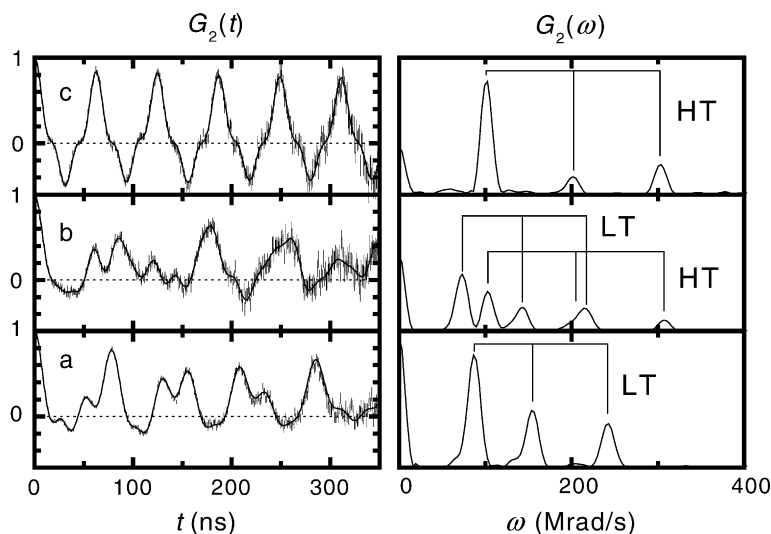


Fig. 1. PAC spectra and Fourier amplitude transforms exhibiting (a) the LT signal at 10.6 °C; (b) a superposition of LT and HT signals at 419.0 °C and (c) the HT signal at 524.0 °C. The LT and HT signals are attributed in the text to LT and HT polymorphs.

exhibits a high-temperature (HT) signal with $\omega_0 = 101.0(1)$ Mrad/s and $\eta = 0$. The spectrum measured at the intermediate temperature 419.0°C (Fig. 1b) exhibits a superposition of LT and HT signals. On the right in Fig. 1 are Fourier amplitude transforms. It can be seen that $\omega_2 < 2\omega_1$ ($\eta > 0$) at low temperature (Fig. 1a) while $\omega_2 = 2\omega_1$ ($\eta = 0$) at high temperature (Fig. 1c). Relative amplitudes of the frequency harmonics of each signal indicate the presence of significant non-random texture such as in a sample composed of a small number of large grains.

The coupling frequency for each signal decreases linearly with increasing temperature, as shown in Fig. 2. Lines indicate results of fits to $\omega_0 = \omega_0(0^\circ\text{C})(1+aT)$, giving $\omega_0(0^\circ\text{C}) = 78.92(6)$ Mrad/s and $a = -2.30(3) \times 10^{-4}^\circ\text{C}^{-1}$ for the LT signal and $\omega_0(0^\circ\text{C}) = 111.4(1)$ Mrad/s and $a = -1.80(3) \times 10^{-4}^\circ\text{C}^{-1}$ for the HT signal. The decreases are attributed to thermal expansion. The asymmetry parameter for the LT signal is plotted versus temperature in Fig. 3. The line is the result of a linear fit with $\eta(0^\circ\text{C}) = 0.320(1)$ and $d\eta/dT = -4.45(8) \times 10^{-4}^\circ\text{C}^{-1}$. The asymmetry parameter of the HT signal was zero in all measurements. Large error bars in Figs. 2 and 3 are associated with small signal fractions.

Determination of the two signal fractions is complicated by the presence of non-random texture because the s_0 terms of the two perturbation functions can not be distinguished. We estimated signal fractions using amplitudes of the precessional harmonics, which can be distinguished. The signal fraction at low-temperature f_{LT} was obtained by multiplying the sum $S_1 + S_2 + S_3$ for the LT signal by a normalization factor that makes $f_{\text{LT}} = 1$ at low temperatures for which there is no HT signal. f_{HT} was calculated in a corresponding way with its own normalization factor. The sum ($f_{\text{LT}} + f_{\text{HT}}$) was generally consistent with 1, indicating that this method for estimating signal fractions was satisfactory.

The temperature dependence of f_{HT} shown in Fig. 4 exhibits hysteresis. Upward-pointing triangles indicate mea-

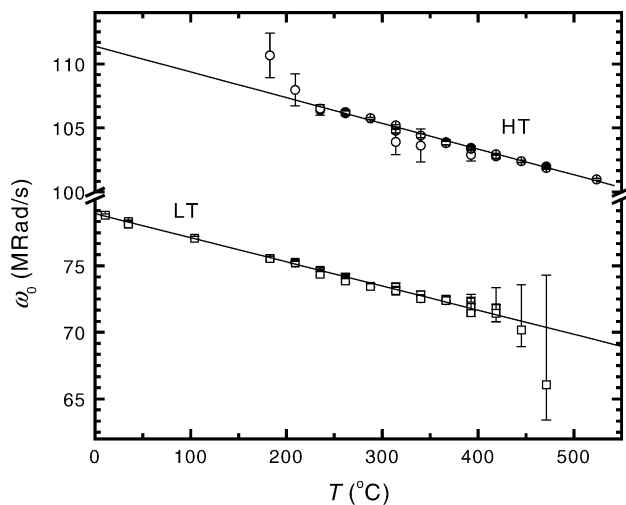


Fig. 2. Temperature dependence of ω_0 for the LT and HT signals.

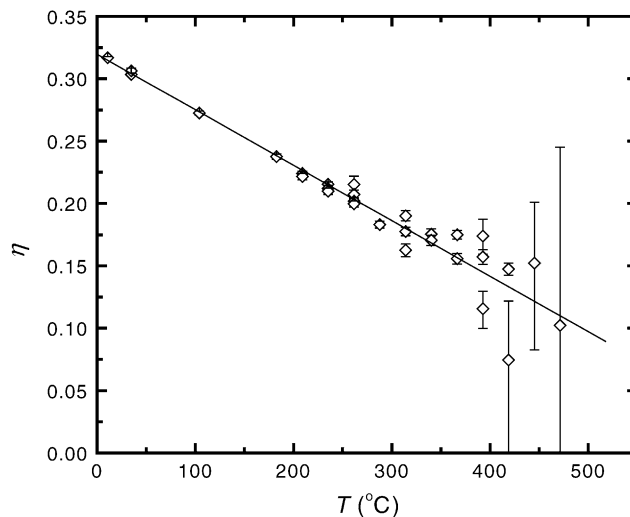


Fig. 3. Temperature dependence of the asymmetry parameter η of the LT signal.

surements after heating and downward-pointing triangles after cooling. Curves indicate approximate limits of the hysteretic temperature range. It was noted that points near the middle of the range were measured after high heating rates ($\approx 0.6^\circ\text{C/s}$) while points close to the curves were measured after low heating rates ($\approx 0.1^\circ\text{C/s}$). Thus, the heating rate between measurements appears to have influenced f_{HT} .

5. Discussion

The non-zero asymmetry parameter η of the LT signal is consistent with the known CeCu_2 structure of In_2La , for which there is a unique In-site having $m..$ -point symmetry. In

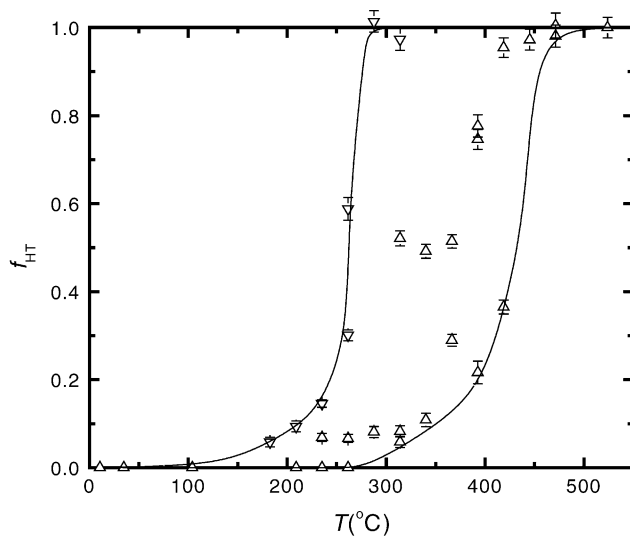


Fig. 4. Site fraction of the HT signal vs. temperature. Upward-pointing triangles indicate measurements made after a heating step; downward-pointing triangles indicate those made after a cooling step.

principle, point defects formed at HT might disturb EFGs at probe nuclei, leading to new signals. In such a case, one would observe inhomogeneous broadening, multiple signals due to different local arrangements of defects, and signals with $\eta > 0$. The HT signal has none of these characteristics and can only represent a new polymorph with higher symmetry ($\eta = 0$). Coexistence of LT and HT phases indicates a first-order phase transformation.

Candidate structures for the HT phase were identified from a survey of MX_2 compounds (M: metal; X: groups IB, IIB, IIIB, IVB elements). Four structures have symmetries at the X site that give $\eta = 0$: AlB_2 , Cd_2Ce , CaIn_2 and MoSi_2 [9]. The structures of Cd_2Ce and CaIn_2 (as well as CeCu_2) can be described as slight distortions of the more symmetrical AlB_2 structure while MoSi_2 has an unrelated structure [10–12]. Examination of the numbers of occurrences of these structures for various metal valences helps to identify the structure of the HT phase. The CaIn_2 structure is considered unlikely because 91% of known representatives are formed between divalent M and trivalent X. Similarly, the Cd_2Ce structure is considered unlikely because 93% of known representatives are formed between trivalent M and divalent X. Neither CaIn_2 nor Cd_2Ce has representatives with trivalent M and trivalent X. The MoSi_2 and AlB_2 structures are observed for wide ranges of M and X valences; however, only AlB_2 has representatives with trivalent M and trivalent X. Further support that the HT structure may be AlB_2 is that both it and the CeCu_2 structures have been observed in the RCu_2 series (R = rare-earth). Cu_2La has the AlB_2 structure at room temperature while the remaining RCu_2 phases have the CeCu_2 structure [13]. Based on these symmetry and chemistry considerations, the most likely structure of the HT phase of In_2La is the AlB_2 structure.

6. Conclusion

A new phase of In_2La that is stable above $\sim 500^\circ\text{C}$ was discovered by quadrupole interaction measurements using perturbed angular correlation of gamma rays. A first-order transformation was observed between low and high tem-

perature phases, which occur with hysteresis in the range $200\text{--}450^\circ\text{C}$. The In-site in the high-temperature phase has higher point symmetry than in the low-temperature phase. Evidence was presented that the high-temperature phase has the hexagonal AlB_2 structure. Other compounds having the CeCu_2 structure at room temperature may transform to a high-temperature structure in the same way as In_2La . For example, recent experiments in this laboratory indicate that such a transformation takes place in CeIn_2 below 524°C .

Acknowledgments

This research was supported in part by the National Science Foundation under grant DMR 00-91681 (Metals Program). ERN is grateful to the Marco Polo Fonds for additional support.

References

- [1] W. Ying, S. Xuping, Y. Fucheng, L. Zhi, W. Xianping, C. Chuntao, *J. Alloys Compd.* 333 (2002) 118–121.
- [2] O.D. McMasters, K.A. Gschneider Jr., *J. Less-Common Metals* 38 (1974) 137–148.
- [3] M.O. Zacate, A. Favrot, G.S. Collins, *Phys. Rev. Lett.* 92 (2004) 225901.
- [4] E. Bodenstedt, U. Ortabasi, W.H. Ellis, *Phys. Rev. B* 6 (1972) 2909.
- [5] H. Frauenfelder, R.M. Steffen, *Alpha-, Beta- and Gamma-ray spectroscopy*, North-Holland, Amsterdam, 1968.
- [6] G. Schatz, A. Weidinger, *Nuclear Condensed Matter Physics*, John Wiley & Sons Ltd, West Sussex, 1996.
- [7] D. Wegner, *Hyperfine Interact.* 23 (1985) 179 (note that the first factor in parentheses in Eq. 5b is incorrect and should be replaced by $(1-\eta^2)$).
- [8] M.O. Zacate, B.C. Walsh, L.S.-J. Peng, G.S. Collins, *Hyperfine Interact.* 136/137 (2001) 653–658.
- [9] P. Villars, L. D. Calvert (Eds.), *Pearson's Handbook of Crystallographic Data for Intermetallic Phases*, second ed., ASM, Materials Park, Ohio, 1991.
- [10] A. Iandelli, A. Palenzona, *J. Less-Common Metals* 15 (1968) 273–284.
- [11] A.C. Larson, D.T. Cramer, *Acta Crystallogr.* 14 (1961) 73.
- [12] P. Svoboda, M. Doerr, M. Loewenhaupt, M. Rotter, T. Reif, F. Bourdarot, P. Bulet, *Europhys. Lett.* 48 (4) (1999) 410–414.
- [13] A.R. Storm, K.E. Benson, *Acta Crystallogr.* 16 (1963) 701.